Target detection in a forest environment using spectral imagery

R. C. Olsen[a], S. Bergman[a], and R. G. Resmini[b],
[a]Physics Dept, Naval Postgraduate School, Monterey, California, 93950
[b]Science Applications International Corp., Chantilly, VA 20151

ABSTRACT

Spectral imagery from the HYDICE instrument was analyzed for the purpose of target detection and identification. Data in the 0.4 - 2.5 micron wavelength range were acquired during the FOREST RADIANCE data collect. Data were analyzed from an area consisting of grassy fields and forest areas. A variety of targets were deployed in the field, with ground truth spectral measurements made. Analysis of reflectance data utilizing "ground truth" and "in-scene" spectra was conducted. The former suffered somewhat from inaccuracies in calibration, but training on subsets of the data allowed for relatively successful detection and classification in the remainder of the data. Spectral angle mapper and matched filter techniques were used. Both were successful in locating targets, but the latter seemed to suffer more from "false positives", though this may have been a function of thresholds set in the classification process.

Keywords: hyperspectral imagery, target detection

1. INTRODUCTION

Imaging spectroscopy has emerged as an important new tool in remote sensing, providing new opportunities to detect and classify materials and targets. Substantial recent progress has occurred with sensors in the visible, near-infrared (NIR) and short-wave-infrared (SWIR) regions. These instruments are defined by their ability to collect reflected solar data over a large number of discrete, contiguous spectral bands or channels. This capability represents a major advance in the collection and exploitation of signature data by providing near-complete spectral coverage of sufficient resolution to identify narrow absorption features of both natural and man-made objects. It is this increased level in spectral resolution that makes the observation of subtle variations in a material's spectrum possible for the first time[1, 2, 3, 4].

A number of field experiments were conducted during the 1994-1997 time period to study the utility of imaging spectrometry. Settings have included, desert, marine, and forested environments. The purpose of these applied remote sensing experiments is to ascertain the utility of the technology to satisfy the Levels of Information (LOIs) identified by each of the services. The experiments are typically executed at a single collection site. Observables typically include overtly exposed, partially exposed, and concealed targets (i.e., vehicles, painted wood, metal, and canvas panels) situated in a target array to facilitate collection and exploitation.

2. EXPERIMENT DESCRIPTION

2.1 Forest Radiance I

Forest Radiance I was the third in a series of collection and exploitation experiments[7]. The intent was to expand upon the knowledge and experience gained from experiments, conducted in CY-94 and CY-95 in desert environments. The Forest Radiance I operation was the program's first attempt at examining the non-linear effects caused by shadow and natural canopies. The Forest Radiance I tests were staged at the Aberdeen Proving Ground's H-Field from 18 to 31 August 1995.

2.1.1 The H-field site

The H-Field Range is located on Edgewood Peninsula approximately 20 miles northeast of Baltimore, MD. The H-Field setting provided three distinct environments in which to deploy the target arrays: 1) a large open field, to deploy a total of 77 completely exposed vehicle and target panels; 2) a road adjacent to both the field and wooded treeline, to ease target re-

deployment and facilitate exploring the non-linear effect due to shadow; and 3) a woodland forest, to evaluate the effects caused by partially concealed objects under canopy.

The H-Field site was specifically selected to provide a realistic forest environment to satisfy four priority Levels-of-Information (LOI) identified for exploitation (e.g., spectral characterization, material identification, subliteral detection, time quantification). H-Field was ideally suited to this experiment because both mobile and fixed objects could be deployed in exposed, shadowed, and canopy areas at a single location. The experiment was executed in three separate phases, each employing a progressive state of concealment. The first phase, Phase I, emphasized a suite of overtly exposed vehicles, decoys, and target panels. In Phase II, the observables were re-deployed to the shadowed area adjacent to the treeline. In Phase III, the objects were again redeployed under canopy for partial concealment. Only data from Phase I are shown in this paper.

Throughout the experiment target spectra, illumination effects, and atmospheric depth were evaluated at three altitudes (5,000, 10,000, and 20,000 ft) and varying sun angles (mid-morning, local noon, mid-afternoon). Varying the overflight altitudes provided data sets with a range of subpixel and multipixel targets, which were comprised of a mixture of target and background material spectra. The primary targets were tracked and wheeled vehicles.

A variety of reflectance calibration targets were deployed to aid radiance calibration to apparent surface reflectance. These calibration panels provided a spectrally near-homogeneous medium in which a baseline spectral library could be established. These facilitated conversion of radiance data to reflectance, as described below. Using both similar and different vehicle types, spectral discrimination between the same target type and between different vehicle classes can be evaluated.

2.1.2 Phase I - Exposed Material and Vehicle Experiments

The first phase of the experiment was conducted from 24-25 August 1995. It emphasized the collection of hyperspectral signature data from unobstructed target panels, vehicles, and fabrics. The fully exposed test area provided a uniform energy distribution on the target array, thus yielding quantitative surface condition results. This test area also provided a near-uniform grass background which enhanced the spectral contrasted between the relevant targets and the natural vegetative background.

US Army Topographic Engineering Center (TEC) ground-truth teams collected over 400 in situ spectral signatures using a GER Field Spectrometer. The measurements of the target panels and vehicles were collected from an average height of 1 m, while the larger fabric materials were sampled using a truck mounted mechanical boom. The reflectance data were collected in the 0.35 - 2.5 μm range and their values calculated relative to the Spectralon 99% reflectance standard. Simple target objects were measured at least three times, while more complex materials were measured several times.

2.2 Sensor characteristics

The Hyperspectral Digital Imagery Collection Experiment (HYDICE) and Airborne Remote Earth Sensor (ARES), two high quality state-of-the-art spectra-radiometers, were selected to make the wide range of spectral measurements designed into the experiment. Only HYDICE data are presented here.

2.2.1 Hyperspectral Digital Imagery Collection Experiment (HYDICE)

The HYDICE sensor was designed and developed by Hughes-Danbury Optical Systems, Inc., to provide high quality hyperspectral data to explore literal and nonliteral exploitation techniques for a wide variety of applications. The sensor is integrated onboard an Environmental Research Institute of Michigan (ERIM) Convair (CV-580) aircraft. The sensor is a nadir-viewing, 210 channel imaging spectrometer covering a spectral range from 0.4 μm to 2.5 μm; visible through the SWIR domain. The spectrum is sampled contiguously in 10 nm wide channels using a pushbroom technique. Light enters the sensor perpendicular to the flight path, and is then dispersed by a prism onto a single array detector. The sensor covers a swath width of approximately 1 km at 20,000 ft AGL, and provides a GSD ranging from 0.75 to 3 m, depending on its operating altitude. Table 1 summarizes the HYDICE sensor's characteristics.

System Attribute	Specification
Platform	ERIM CV-580
V/H (aircraft limits)	0.0127 - 0.059 rad/sec
Optics	Paul Baker foreoptics Schmidt prism spectrometer
Aperture diameter	27 mm
System f/number	3.0
Swath FOV	8.94°
Swath width	208 pixels
IFOV	0.507 mrad (average)
Array size	320 X 210 pixels
Integration time	10.5 msec (design point); 1.0 - 42.3 msec (range)
Frame time	17.3 msec (design point); 8.3 - 50 msec (range)
Readout time; Quantization	7.3 msec (fixed); 12 bits
Spectral co-registration (smile)	5% of FWHM (average)
Spatial co-registration	55 μrad at edge of field (average)
Channel width (FWHM)	7.6 - 16 NM
Instrument operating temperature	10 °C
MTF (laboratory)	> 0.58 in-track; > 0.33 cross-track
InSb focal plane in three regions	A: 0.40-1.0 μm; B: 1.0-1.9 μm; C: 1.9-2.5 μm
Average SNR (by gain region)	217/107/40 @ 5% reflectance
Average dynamic range (by gain region)	955/54/17 watts per m^2/steradian/micron
Polarization	< 4% above 445 nm; < 12% below 445 nm
Spectral transmission @ ∓ 1 FWHM @ ∓ 2 FWHM @ ∓ 4 FWHM	3 - 13% 0.1 - 1.2% 0.02 - 0.6%

Table 1. HYDICE Sensor Characteristics.

3. DATA PROCESSING

3.1 Post-Flight Processing

The raw data are converted to at-sensor radiance following procedures developed in the first year of operation. The conversion of the data from instrument DN to calibrated radiance levels was done prior to analysis, using the best calibration coefficients available as of Spring 1996. Aldrich et al. give more detailed information concerning the radiometric calibration technique[8].

3.2 Reflectance Conversion

The work reported here was all done in the reflectance domain. Utilization of "known" spectra in target location generally requires conversion from at-sensor radiance to apparent reflectance. The Empirical Line Method was used here to convert the radiance data sets to apparent surface reflectance. This process eliminates the effects of errors in conversion to radiance.

3.3 Empirical Line Method (ELM)

The correction of the HYDICE data to apparent reflectance was accomplished using the Empirical Line Method (ELM). The ELM converts the radiance data to an apparent surface reflectance based on the internal characteristics of the data set. This method requires a prior knowledge of the target area, and each scene must include a minimum of two regions (e.g., calibration panels) with a broad range of reflectance values. Ground-truth-derived spectra of the calibration panels are necessary and must also be acquired in the field. The next step is to manually select pixels from the scene that correspond to each target region to record their apparent reflectance values. A linear regression is then calculated to determine the gains and offsets for each band (wavelength) in the image cube. Next, the offset value is subtracted from the data in order to deal with scattering, absorption, and attenuation effects caused by the atmosphere. The final step is to divide the sensor-derived DN values by the calculated gain. This technique, while not perfect, does facilitate comparisons between remotely sensed spectra and field- or laboratory derived spectral signatures[9].

4. FOREST RADIANCE

4.1 Objectives

The H-Field range was divided into separate target areas to maximize probability of success for each individual mini-experiment. To satisfy the broad range of objectives, a wide array of target objects of varying shapes, sizes, and material types were deployed in different orientations throughout the test area. The primary objective of this report is to ascertain the utility of hyperspectral data and exploitation techniques to detect and discriminate the spectral signatures of exposed mobile vehicles, against the natural grass background. A thorough examination of the spectral variability inherent in these objects and on-line target and anomaly detection methods was conducted. This report defines an anomaly as a target of military interest.

4.2 Forest Radiance I Data Set

A HYDICE-derived hyperspectral image scene was selected from: Run 05, major frames 51-54, acquired on 950824 at an altitude of 5,000 ft above ground level (AGL) at 0910 local time (LT). This flight line provides 0.75m ground sample distance (GSD). Target spectra were either sampled directly from the image cubes being analyzed or selected from in situ-derived ground-truth measurements. A total of thirty nine (39) target signatures were selected for processing. For the work shown here, five (5) mean spectra were derived by averaging four (4) pixels from each of the 5 vehicles (targets) of interest. This averaging technique was employed because exposed target pixels are rarely homogeneous and averaging compensates for some of the compositional heterogeneity.

Figure 1 is shown here to orient the reader and establish target position of the overtly exposed vehicles arrayed during the first phase of the experiment. All vehicles relevant to this investigation are prominently displayed and labeled to the right of the target array. Note that it would be difficult to identify the vehicles in a mono-chromatic image such as the one found here.

4.3 Methodology/Approach

A Principal Components Analysis (PCA) was first applied to the image cube to estimate the inherent dimensionality of the data sets being analyzed. This intrinsic dimensionality does not correspond to the exact number of bands in the data set since scenes typically have significant correlation between image bands. The intent is to compress the information content of the data set into a relatively few principal component (PC) bands. Though primarily useful as a diagnostic process, or a precursor to more involved techniques, PC analysis can be effective as a stand-alone technique[10, 11, 12]. Low Probability of Detection (LPD)[13, 14] and Spectral Angle Mapper (SAM)[15] target and anomaly detection techniques were then applied to physically highlight pixels found to have similar spectral characteristics as the target spectra. The LPD and SAM algorithms required the selection of an endmember spectra as a target signature, with the remaining image spectra being undesired. The search methods yield a resultant match relative to this target signature. Detection is then based on a (somewhat arbitrary) threshold of that measure.

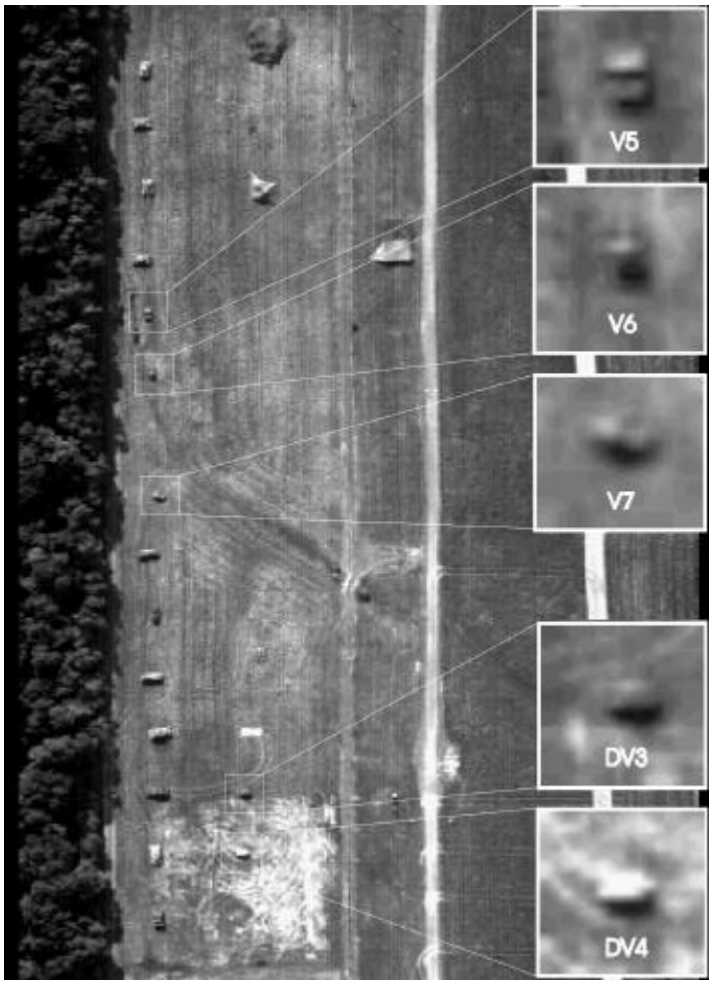

Figure 1. Forest Radiance scene, H-field, primary targets (vehicles). (Band 33, 529 μm)

5. ANALYSES

The LPD and SAM processing techniques serve to compress the data set being analyzed. The number of bands in the output cube is equal to the number of target materials considered. All of the target spectra were acquired directly from the image scene. The results to be presented demonstrate the robustness of these techniques in detecting and discriminating two classes of vehicles. Here targets V5, V6, V7 form one homogenous group, and are to be distinguished in particular from the target designated here as DV4.

5. 1 Qualitative analysis of signatures

A primary element which arose from this work was the substantial variability which appears in the targets illustrated in Figure 1. Figure 2 shows the scene-derived spectra taken from V5. The spectra exhibit a chlorophyll response similar to that found in the natural grass background. There are two plausible explanations for this very curious phenomenon. One possibility is that the materials used in the paint were manufactured to mimic natural vegetation in that portion of the spectrum. It is also feasible that the sensor recorded the photons that had first reflected off the adjacent tree-line or the surrounding grass before interacting with the vehicle. Further notice the significant amount of variation in the four spectra.

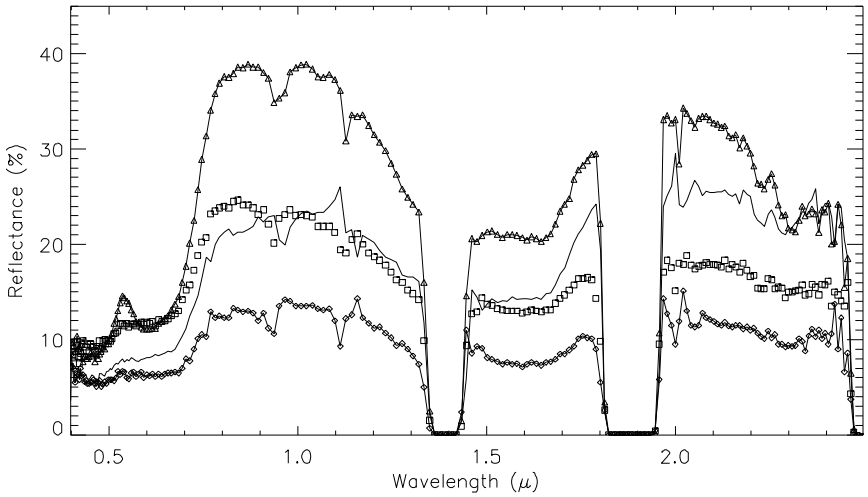

Figure 2. Hydice Spectra from Target V5

Table 2 is provided to characterize V5's intra-spectral relationship, using as a measure correlation coefficients. Note that the self-correlation values for the spectra range from 0.86 to 0.96. These statistical variances could be attributed to either the complex signature associated with the paint schemes, but may also be the result of specular scatter. An interview with one ground-truth team member indicated that the paint in the bed of at least one vehicle was extremely worn and the underlying metallic material was clearly exposed. Glint may have also resulted from solar energy reflecting off the windows of the vehicle.

	Spectra 1	Spectra 2	Spectra 3	Spectra 4
Spectra 1	1.00	0.89	0.93	0.86
Spectra 2		1.00	0.94	0.95
Spectra 3			1.00	0.96
Spectra 4				1.00

Table 2. Correlation Coefficients Associated With Spectra From V5

Similar variability is found in the ground measurements of the same target (not shown). The correlation coefficients associated with these spectra vary from 0.83 to 0.96. The ground-truth-derived spectra were not used further in the analyses.

The spectral response fluctuates to some degree within each of the target objects. To compensate for these variations in the spectra an averaging technique was applied to calculate a mean spectrum for each vehicle. This approach was considered necessary in order to decrease the probability of false alarms later in the analyses.

Figure 3 combines these mean spectra into a single figure to illustrate the spectral diversity within each natural and man-made target class. V7's mean spectral signature is almost identical to V5 and has been omitted from the plot to avoid cluttering the figure. The individual spectra are labeled and displayed with an offset value (+12) to assist the reader in discerning the inherent characteristic associated with each spectrum under examination. Table 3 lists the correlation coefficients associated with these spectra. Note that the correlation between targets (average spectrum) is higher than most of the values shown in Table 3 for target V5. There are some minor problems evident in the figure. In particular, the local minimum at 0.94 microns (μm) is an atmospheric feature which has not been properly dealt with in the atmospheric

	DV4	Grass	V5	V6
DV4	1.00	0.96	0.97	0.96
Grass		1.00	0.99	0.98
V5			1.00	0.99
V6				1.00

Table 3 Correlation coefficients for mean spectra

correction.

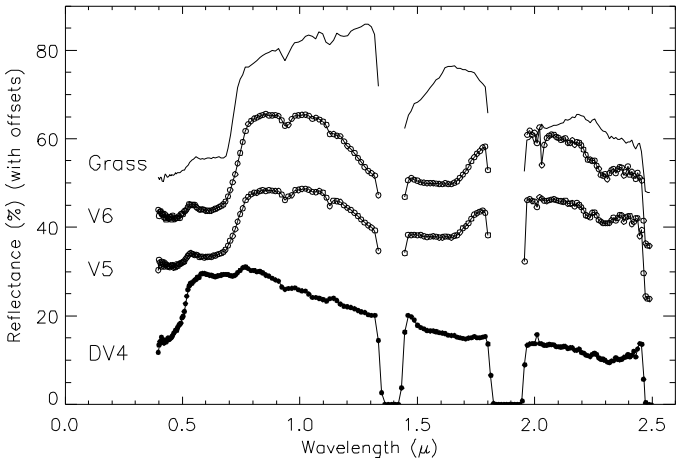

Figure 3. Means of target spectra, and background (grass)

5.1 Principal Components Analysis (PCA)

The data set was first investigated using the Principal Components Analysis method. Figure 4 shows bands 1, 4, and 5 of the transformed reflectance data. The first component (band 1, in blue here) is the scene brightness. The next four or five bands highlight spectral differences. Clearly this has analytical benefits since bands one, four, and five highlight the man-made objects in the target array. The remaining, higher order bands are dominated by noise and sensor artifacts. No further comment is made on the PCA results, per se.

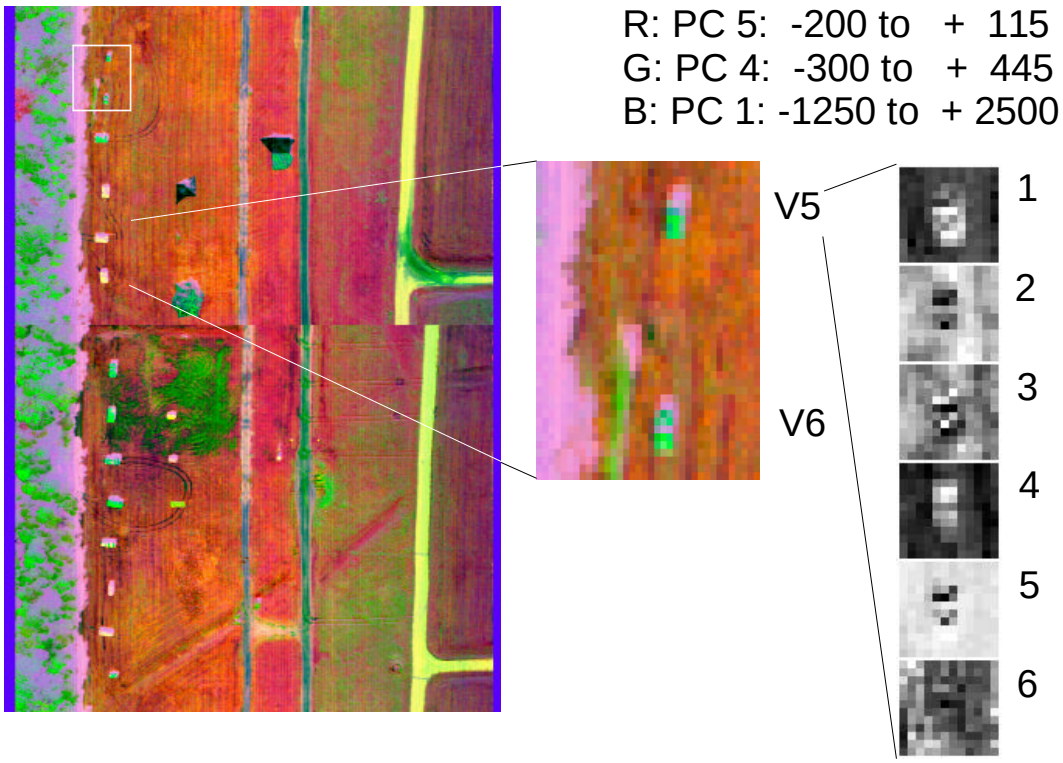

Figure 4. Results from PCA, 2% histogram stretch. Scaled dynamic range of each band is indicated. The first 6 principal component images are shown for the V5 target region.

The principal components analysis is viewed next as a pre-cursor to the utilization of the LPD algorithm, which requires some knowledge of the intrinsic dimensionality of the scene - and in particular the background elements of the scene. (Stefanou provides a fairly complete analysis of this aspect of the LPD algorithm [15].) A fairly straightforward approach is to plot the eigenvalues of the PC transform variance, and look for the characteristic 'break' in the curve, which in HYDICE data typically occurs around band 10 or 15. Such a plot for these data (not shown) indeed shows a transition at about band 10; well over 99% of the variance in the scene can be expressed by the first 10 bands of the PC transformed reflectance cube.

5. 2 Low Probability of Detection (LPD)

The performance of the Low Probability of Detection (LPD) method depends on the inherent dimensionality of the data set being analyzed. The technique begins by forming a basis set of eigenvectors which characterizes the majority of the scene spectral elements (the background). A filter vector is then formed from these eigenvectors, and the desired (target) pixel vector, and applied to the scene. The LPD algorithm was applied here in an attempt to discriminate two classes of similar vehicles, and those of unknown man-made or natural background materials. Scene-derived spectra of V5, V6, V7, DV3 and DV4 were selected as target signatures and fifteen eigenvectors were selected to characterize the scene's (background) variability. This number was chosen to ensure that most of the undesirable background signatures would be suppressed during the analyses. The results from analysis using the average spectrum from target V5 are shown in Figures 5 and 6.

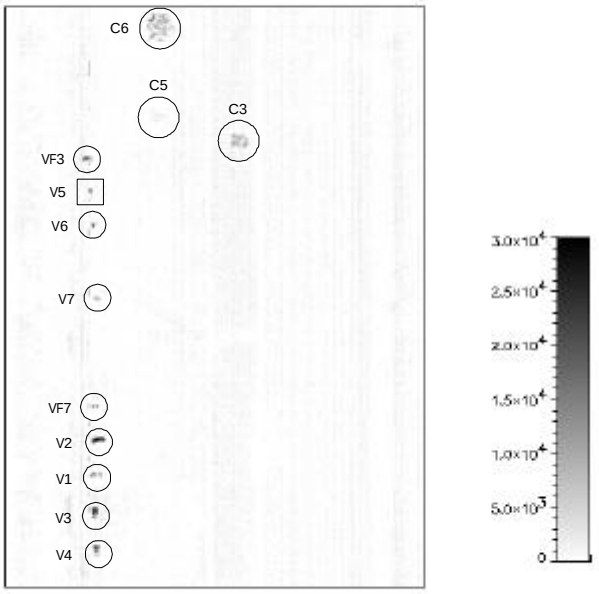

Figure 5. LPD results using average spectrum from target V5.

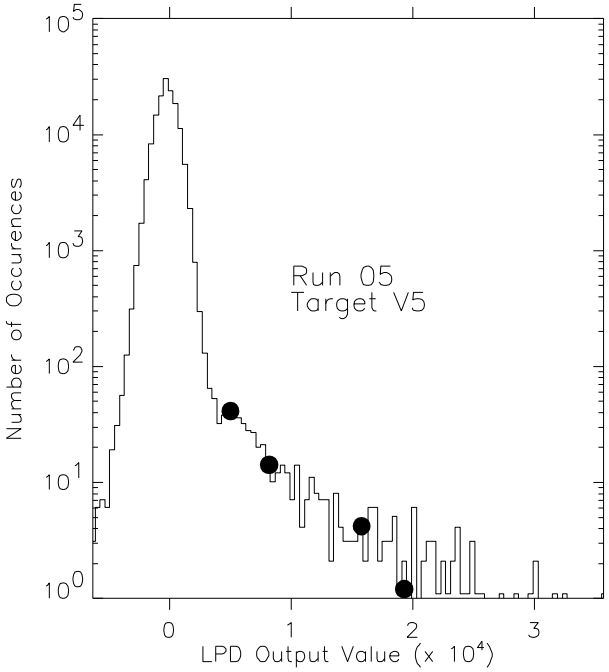

Figure 6. Histogram of results from LPD analysis.

The output from the algorithm is a pixel value ranging, in this case, from ~ -5,000 to ~ +35,000. These scaled pixel values are nominally proportional to the material abundance, at least in the original geophysical application [13]. Here, the man-made targets are generally well separated from the background, including the fabric panels (C3, C5, C6). The target spectrum is highlighted, as expected (the boxed pixels in Figure 5). The vehicle designated DV4 is not highlighted. Still, the output values for the desired target are not, in general, the largest output values, as indicated by Figure 6. In this figure, the output for the 4 target pixels used to construct the mean V5 spectrum are indicated by small black dots. A number of other elements in the scene obviously give responses which are as large or larger than the target. This high number of "false alarms" on other man-made objects appears to be a ubiquitous feature of all the projection and rotation techniques [14]. Note that if a specific target pixel is used, instead of the average, results very similar to those shown in Figure 6 occur, so the results shown in Figures 5 and 6 are not a consequence of using the mean spectrum.

Using a different target (V6 or V7) provides very similar results (not shown here). The distribution of data values is very similar to that found for target V5. Differences did appear when using the LPD algorithm with the DV4 target spectrum (not shown). The DV4 target was highlighted; targets V5 and V6 were not selected.

The results of the applied algorithm indicates that spectral separability between two vehicle classes is possible. When the LPD algorithm was run with V5, V6, and V7 as target spectra, neither DV3 nor DV4 flagged as false alarms. There was, however, a significantly high false alarm rate with the various vehicles deployed in the array, which is indicative of a strong spectral correlation. The similar spectral shape of the vehicles clearly attributed to their misidentification.

Unfortunately, the fabrics situated at the end of the target array were also flagged as false alarms. This phenomenon demonstrates a significant response among fabrics and vehicles sporting green paint schemes. Vehicles with differing paint schemes in general did not cause false alarms.

5. 3 Spectral Angle Mapper (SAM) Results

The Spectral Angle Mapper (SAM) technique was applied to the same data set using the same overall approach employed in the LPD analyses. Target objects V5, V6, V7, DV3, and DV4 were used as target spectra. The SAM algorithm is applied by (effectively) taking the dot product of the spectrum at each pixel with the target spectrum. The resulting ensemble of angles is presented as a gray scale image, scaled here from 0.0 and 0.3 radian (17 °). Classification is done by thresholding the results at a smaller angle, here defined as 0.1 radian (5.7 °). Objects that have spectra nearly identical to the target spectra will pass the selection criteria (< 0.1), and will be colored black. The remaining pixels are colored white.

The results are similar to those found with the LPD algorithm. The man-made targets, and in particular the vehicles, fairly uniformly produced small spectral angles. The outputs for the 4 pixel vectors utilized in constructing the target vector are again indicated in the histogram by black dots. (Two occur at 7 °.) Note that if a single pixel from the target had been used as an input to the SAM algorithm, there would have been one occurrence at 0 °. Using the mean spectrum, the smallest response was 2.6°.

The number and location of the false alarms are nearly-identical to those found in the LPD analyses, using a threshold angle of 0.1 radian. Attempts to reduce the false alarm rate by incrementally reducing the threshold angle had little effect on the final output. The findings indicate that spectral discrimination between the two target classes is possible using this technique. When the SAM algorithm was applied using V5, V6, and V7 as target spectra, neither DV3 nor DV4 appeared as false alarms.

The absence of false alarms on the fabrics is the most obvious feature missing in the SAM classifiers. The fabrics, roads, and a bare patch of ground near the bottom of the scene occur at spectral angles above the threshold in this case. For example, the output for the soil pixels seem to range from about 11 to 14 degrees.

The SAM algorithm was also applied to the data cube using DV4 pixels as target spectra. None of the target vehicles or fabrics false alarmed in the SAM classifier. Several of the man-made objects did, however, give responses between 0.1 and 0.3 radians.

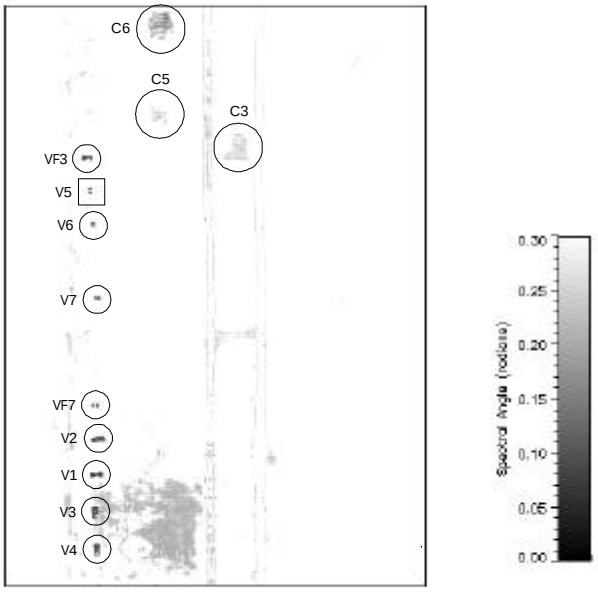

Figure 7. SAM results using average spectrum from target V5 spectrum.

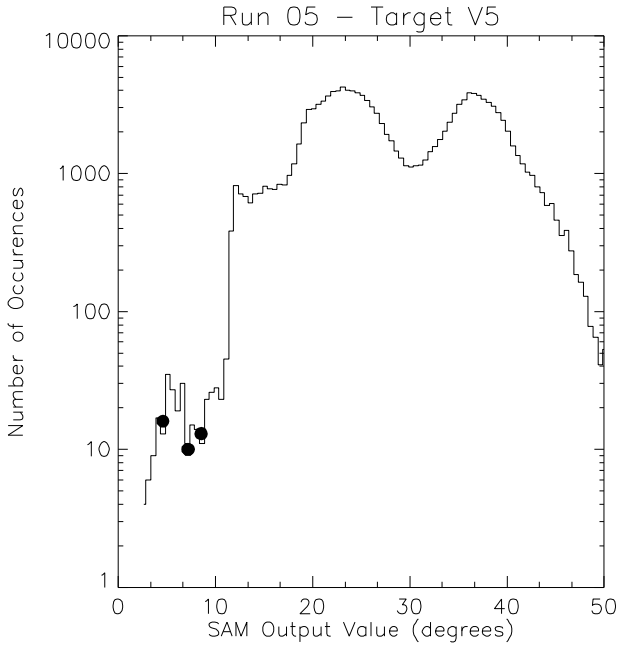

Figure 8. Histogram of results from SAM analysis.

6. SUMMARY AND CONCLUSIONS

The purpose of the analysis illustrated here was to determine the effectiveness of three standard spectral analysis techniques in distinguishing between two classes of vehicles in the forest environment. All of the techniques shown here were effective in distinguishing between the man-made targets and the chlorophyll dominated background. The LPD and SAM algorithms were both successful in distinguishing between the vehicle classes. There are false-alarm problems with these techniques, however. It appears that more refined approaches are needed. One such would be to use the LPD algorithm to identify anomalous targets, and then additional techniques to separate the small subset of pixels obtained in this way. M. Pilati from the USAF/NAIC has been pursuing such techniques [16].

7. ACKNOWLEDGEMENTS

Thanks go to the Spectral Imagery Technology Applications Center (SITAC) for providing the data utilized for this study.

8. REFERENCES

1. Goetz, A.F.H., Vane, G., Soloman, J.E., and Rock, B.N., Imaging Spectrometry of Earth Remote Sensing, *Science*, Vol. 228, No. 4704, pp. 1147-1153, June 1985.

2. Vane, G., First Results from the Airborne Visible/ Inrared Imaging Spectrometer (AVIRIS), *Proceedings of the International Society for Optical Engineering (SPIE)*, Vol. 834, pp. 166-174, August 1987.

3. Vane, G., and Goetz, A.F.H., Terrestrial Imaging Spectroscopy, *Remote Sensing of the Environment*, Vol. 24, pp. 1-29, February 1988.

4. Kruse, F.A., Use of the Airborne Imaging Spectrometer Data to Map Minerals Associated with Hydrothermally Altered Rocks in the Northern Grapevine Mountains, Nevada, California, *Remote Sensing of the Environment*, Vol. 24, No. 1, pp.31-52, February 1988.

5. Fulghum, D.A., Predators Bound For Bosnia Soon. *Aviation Week and Space Technology*, pp. 72-73, November 1995

6. Fay, M.E., An Analysis of Hyperspectral Imagery Data Collected During Operation Desert Radiance , Masters Thesis, Naval Postgraduate School, Monterey, CA., June 1995.

7. Anderson, M., Forest Radiance I, Collection and Exploitation Operations Plan, SITAC, 1995.

8. Aldrich, W.S., Kappus, M.E., Resmini, R.G., and Mitchell, P., HYDICE Post Flight Data Processing, *Proceedings of the International Society for Optical Engineering (SPIE)*, Vol. 2758, pp. 354-363, 9-11 April 1996.

9. Farrand, W.H., A Comparison for Retrieving Apparent Surface Reflectance from Hyperspectral Data, *Proceedings of the International Symposium on Spectral Sensing Research (ISSSR)*, Vol. 2, pp. 1154-1164, 1992.

10. Richards, J.A., Remote Sensing Digital Image Analysis , New York: Springer-Verlag, 1995.

11. Johnson, P.E., Smith, M.O., and Adams, J.B., Quantitative Analysis of Planetary Reflectance Spectra with Principal Components Analysis, *Proceedings of the 15th Lunar and Planetary Science Conference, Part 2, Journal of Geophysical Research*, Vol. 90, pp. C805-C810, February 1985.

12. Molinelli, E., and Muncill, G., Use of Principal Components to Characterize Upwelling off the Coast of California, *Proceedings of the International Symposium on Spectral Sensing Research (ISSSR)*, Vol. 2, pp. 707-710, July 1994.

13. Farrand, W.H., and Harsanyi, J.C., Discrimination of Poorly Exposed Litologies in Imaging Spectrometer Data, *Journal of Geophysical Research - Planets*, pp. 1565-1578, 1995.

14. Harsanyi, J. C., Detection and Classification of Subpixel Spectral Signatures in Hyperspectral Image Sequences, PhD thesis, University of Maryland, 1993.

15. Stefanou, M. S. A Signal Processing Perspective Of Hyperspectral Imagery Analysis Techniques, Masters Thesis, Naval Postgraduate School, Monterey, CA, June, 1997.

16. Wolboldt, M., M. Pilati, and D. L. Perry, Hyperspectral detection algorithms for VIS-SWIR sensors, SPIE, 1997, paper 3118-31.

Further author information -
R.C.O. (correspondence): Email: olsen@physics.nps.navy.mil